Optical Imaging:

3D Approximation and Perturbation Approaches

for Time–domain Data

Regine Model, Matthias Orlt, Monika Walzel

Physikalisch–Technische Bundesanstalt
Abbestraße 2–12, D–10587 Berlin, Germany

Rolf Hünlich

Weierstrass Institute for Applied Analysis and Stochastics
Mohrenstraße 39, D-10117 Berlin, Germany

Abstract

The reconstruction method presented here is based on the diffusion approximation for the light propagation in turbid media and on a minimization strategy for the output-least-squares problem. A perturbation approach is introduced for the optical properties. Here, the number of free variables of the inverse problem can be strongly reduced by exploiting a priori information such as the search for single inhomogeneities within a relatively homogeneous object, a typical situation for breast cancer detection. Higher accuracy and a considerable reduction of the computational effort are achieved by solving a parabolic differential equation for a perturbation density, i.e. the difference between the photon density in an inhomogeneous object and the density in the homogeneous case being given by an analytic expression. The calculations are performed by a 2D FEM algorithm, however, as a time-dependent correction factor is applied, the 3D situation is well approximated. The method was successfully tested by the University of Pennsylvania standard data set. Data noise was generated and taken into account in a modified data set. The influence of different noise on the reconstruction results is discussed.

I. INTRODUCTION

The development of optical tomographic methods has been of strongly increasing interest in the last few years because of its potential for applications in medical diagnostics, for example, cancer detection in the female breast [1]. Malignant tumors may cause changes in the optical properties as compared with the surrounding normal tissue. The shapes of time-of-flight curves in time-resolved measurements are affected by the spatially dependent optical properties of the transilluminated tissue object. They carry information about changes in absorption and changes in the scattering properties and hence about possible pathological alterations. Near infrared light (NIR) transilluminations are attractive because the risk of radiation damage due to ionizing radiations is avoided. As biological tissue is a strongly scattering medium, after propagation through tissue, light is diffuse so that image reconstructions are more difficult. Consequently, there is a strong demand for the development of effective reconstruction methods. Recently, imaging algorithms for different measurement types were published [2–7]. Sufficiently accurate simulation of light transport (forward problem) is a prerequisite for solving the inverse problem in optical tomography. On weak assumptions, the light propagation in scatter-dominated media can be modeled as a diffusion process [8]. In the case of time-resolved measurements, a parabolic differential equation for the photon density has to be solved. The application of a numerical method such as the finite-element method (FEM) allows different geometries and parameter distributions to be taken into account.

The aim of this paper may divided in five parts, all serve the intention to develop an effective imaging reconstruction algorithm. (i) In general, because of the computational effort of FEM-calculations a three-dimensional treatment is very expensive. The problem is to find an algorithm for 3D-data using 2D-FEM. (ii) Nevertheless, the 2D-simulations

1

must be fast and accurate. (iii) An improvement of the usually bad condition of the inverse problem and a reduction of the effort could be reached by exploiting a priori information. (iv) The algorithm is tested by general available data series [13] as a step toward comparisons between different imaging algorithms. (v) In further tests data noise has to be considered for more realistic situations.

A higher accuracy for the forward simulation and a considerable reduction of the computational effort are reached by solving a partial differential equation for the difference between the time-dependent photon density in an inhomogeneous object and the density in the homogeneous case given by an analytic expression. The equation for the perturbation is derived in Section II A, first for an infinite medium. Perturbation approaches are in general an appropriate tool in case of small changes of parameters and they are used in the field of optical tomography for both continous wave and frequency modulation conditions [9–12]. The calculations are performed by a 2D FEM algorithm, but as a time-dependent correction factor is applied, the 3D situation is well approximated. In Section II B, comparisons are made between the University of Pennsylvania standard data set [13] and forward simulated data as described in Section II A. The numerical treatment of the problem in two spatial dimensions with subsequent correction by a time-dependent factor leads to substantial reductions of the computational effort compared with three-dimensional calculations. The simulation of noise [14] is used to obtain more realistic data.

On the basis of the diffusion model the imaging problem then becomes an identification problem of partial differential equations with distributed parameters. A reconstruction method will be introduced in Section III A, which allows all the information contained in the time-resolved measurement data to be exploited. It combines the forward simulation procedure with a weighted least squares technique. The number of free variables of the inverse problem can be reduced by exploiting a priori information such as the search for single inhomogeneities within a relatively homogeneous object, a typical situation for breast cancer detection. The influence of the data noise and of the source-detector configuration on the reconstruction results will be discussed in Section III B.

II. THE FORWARD MODEL

A. Mathematical model

Light propagation in highly scattering media may be described by the widely used diffusion approximation of the Boltzmann transport equation, which leads to the parabolic differential equation for the photon density Φ

$$\frac{\partial}{\partial t} \Phi(\boldsymbol{x}, t) = \operatorname{div}\left(D(\boldsymbol{x}) \operatorname{\mathbf{grad}} \Phi(\boldsymbol{x}, t)\right) - c\,\mu_a(\boldsymbol{x})\,\Phi(\boldsymbol{x}, t) + s(\boldsymbol{x}, t), \quad \boldsymbol{x} \in \Omega, \;\; 0 < t \le T. \quad (1)$$

Here c is the speed of light in the medium, $\mu_a(\boldsymbol{x})$ the absorption coefficient and $s(\boldsymbol{x}, t)$ a source term. The optical diffusion coefficient is

$$D(\boldsymbol{x}) = \frac{c}{3\left(\mu_a(\boldsymbol{x}) + \mu'_s(\boldsymbol{x})\right)}$$

2

where $\mu'_s(\boldsymbol{x})$ is the reduced scattering coefficient. The boundary conditions for a finite medium are derived from the Boltzmann equation in the same way as the diffusion equation [8]. The result is a condition of the third kind

$$- D(\boldsymbol{x}) \frac{\partial \Phi(\boldsymbol{x}, t)}{\partial \boldsymbol{n}} = c\, h(\boldsymbol{x})\, \Phi(\boldsymbol{x}, t), \quad \boldsymbol{x} \in \partial\Omega, \quad 0 < t \leq T.$$

The boundary parameter h may be determined by an identification procedure [15]. In an infinite medium in which we are interested here, the condition

$$\frac{\partial \Phi(\boldsymbol{x}, t)}{\partial \boldsymbol{n}} \to 0 \quad \text{if} \quad |\boldsymbol{x}| \to \infty, \quad 0 < t \leq T \tag{2}$$

is to be used. For completeness, an initial condition $\Phi(\boldsymbol{x}, 0) = \Phi_0(\boldsymbol{x})$ must be given. The light source may be described in two ways, firstly by the photon source term $s(\boldsymbol{x}, t)$ in equation (1) and, secondly, by the initial function $\Phi_0(\boldsymbol{x})$ corresponding to a δ–pulse in time. For short light pulses, as they are considered here, the results are approximately the same. We prefer to consider the light source as the initial condition, especially in the form of a δ–distribution in space,

$$\Phi(\boldsymbol{x}, 0) = \Phi_0(\boldsymbol{x}) = Q\, \delta(\boldsymbol{x} - \boldsymbol{x}_s), \quad \boldsymbol{x} \in \Omega \tag{3}$$

where $\boldsymbol{x}_s$ and Q denote the source position and the total number of photons in Ω for $t = 0$, respectively.

In general Ω has to be considered as a three dimensional domain. In the following we use a two dimensional formulation of the initial boundary value problem $(1) - (3)$. This problem is solved by a 2D FEM code which is an effective tool even for complicated geometries and arbitrary distributions of the optical properties. The calculation time required to solve a single forward problem substantially influences the computational effort needed for solving an imaging problem because the calculation must be repeated several times. The light source as a δ-pulse in time and space leads to steep gradients in an initial time interval. Consequently, the time steps within this interval have to be small and the grid around the source position has to be very fine to decrease the numerical error. A new perturbation approach will improve this situation. Let us assume that the absorption and the scattering coefficients are constant except for spatially small perturbations. Then the diffusion coefficient D and the absorption coefficient μ_a may be written as

$$D = D_0 + D_1, \quad \mu_a = \mu_{a0} + \mu_{a1} \tag{4}$$

where D_0 and μ_{a0} are constant optical properties and D_1 and μ_{a1} local perturbations. If (4) is taken into account in the diffusion equation (1) and the source term is omitted, we have

$$\frac{\partial}{\partial t} \Phi - \operatorname{div}\left((D_0 + D_1)\, \mathbf{grad}\, \Phi\right) + c\,(\mu_{a0} + \mu_{a1})\, \Phi = 0. \tag{5}$$

The diffusion equation with constant coefficients D_0 and μ_{a0} reads as

$$\frac{\partial}{\partial t} \Phi_c - \operatorname{div}\left(D_0\, \mathbf{grad}\, \Phi_c\right) + c\, \mu_{a0}\, \Phi_c = 0. \tag{6}$$

3

Both densities, Φ and Φ_c, must satisfy the same boundary and initial conditions (2), (3). The 2D solution to (6), (2), (3) is known in analytic form,

$$\Phi_c(\boldsymbol{x}, t) = \Phi_{an}^{2D}(\boldsymbol{x}, t) = \frac{Q}{4\pi D_0 t} \exp\left(-\frac{|\boldsymbol{x} - \boldsymbol{x}_s|^2}{4 D_0 t} - c \mu_{a0} t\right). \tag{7}$$

We now introduce a new function, Ψ, as the difference between the photon density in an inhomogeneous object and the density in the homogeneous medium, both in two spatial dimensions

$$\Psi = \Phi^{2D} - \Phi_{an}^{2D} \tag{8}$$

which satisfies the following equation, i.e. the difference between equations (5) and (6),

$$\frac{\partial}{\partial t} \Psi - \operatorname{div}\left((D_0 + D_1)\operatorname{\mathbf{grad}}\Psi\right) + c\left(\mu_{a0} + \mu_{a1}\right)\Psi = \operatorname{div}\left(D_1 \operatorname{\mathbf{grad}}\Phi_{an}^{2D}\right) - c\mu_{a1}\Phi_{an}^{2D}. \tag{9}$$

A general analytic solution to equation (9) is not known, and a numerical solution is restricted to bounded domains and requires that boundary conditions be given. On the assumption that the perturbation of the optical parameters is small, at a sufficient distance from the perturbations, Φ and Φ_c have approximately the same values. Therefore, homogeneous Dirichlet conditions

$$\Psi(\boldsymbol{x}, t) = 0, \quad \boldsymbol{x} \in \partial\Omega, \quad 0 < t \leq T$$

can be assumed for a sufficiently large domain Ω. Since Φ^{2D} and Φ_{an}^{2D} satisfy the same initial conditions,

$$\Psi(\boldsymbol{x}, 0) = 0, \quad \boldsymbol{x} \in \Omega$$

is valid. Ψ is a slowly varying function with clearly non-zero values close to the perturbation region only. In order to get Φ^{2D} at the detector positions, Φ_{an}^{2D} is calculated and added to Ψ. The absence of steep gradients considerably reduces the computational effort.

The analytic solutions in a homogeneous infinite medium in two and in three spatial dimensions (Φ_{an}^{2D} and Φ_{an}^{3D}) differ by a time-dependent factor

$$\Phi_{an}^{3D} = \frac{1}{2\sqrt{\pi D_0 t}} \Phi_{an}^{2D}. \tag{10}$$

If the perturbations of the optical properties are small, the factor $(2\sqrt{\pi D_0 t})^{-1}$ may be used to approximate the solution of the perturbed 3D problem

$$\Phi^{3D} \approx \frac{1}{2\sqrt{\pi D_0 t}} \Phi^{2D} = \Phi_{an}^{3D} + \frac{1}{2\sqrt{\pi D_0 t}}\Psi. \tag{11}$$

Approach (11) involves two inaccuracies. The first one is the inaccurate correction factor for the perturbed medium, and the second is due to the fact that a bounded 3D inhomogeneity is replaced by a cylinder unbounded in the third coordinate. The resulting error can be reduced in the following way. For the 2D calculations the absorption coefficient or the scattering coefficient of the inhomogeneity is not set to a constant value, but to the changed value valid only in the centre of the inhomogeneity, and to the background value on its boundary. In between, the coefficient is linearly interpolated. This procedure leads to substantially better agreement with real 3D data. It can possibly be further improved.
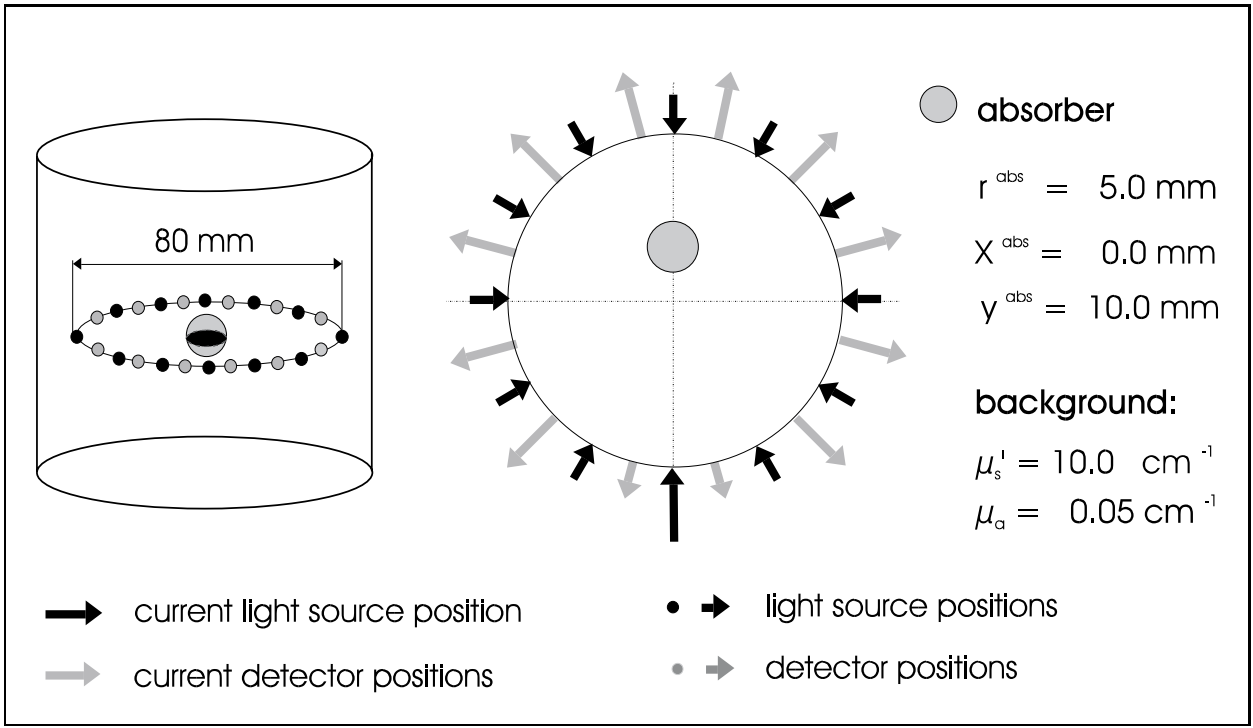
4

Fig. 1: 3D measurement geometry. 12 sources and 12 detectors are positioned in a plane on a circular curve 8 cm in diameter. Background absorption $\mu_a = 0.05\,\mathrm{cm}^{-1}$ and scattering $\mu_s' = 10.0\,\mathrm{cm}^{-1}$.

B. Simulations

First, comparisons are made between data generated by our forward simulator and the University of Pennsylvania standard data set. The standard data were simulated in the frequency domain by an analytic solution [16] assuming an infinite medium with a single absorbing sphere with a different absorption coefficient per series. Time-resolved data have been obtained by subsequent Fourier transformation. The source and the detector arrangement are illustrated in Figure 1. The source is positioned in 12 different locations in a plane on a circle 8 cm in diameter (every 30 degrees) with its centre at the origin. For each source there are 10 detectors which are displaced in intervals of 30 degrees plus an initial 45 degrees from the source. This results in a total of 120 independent time domain measurements of the photon density. The sphere is positioned at $x = 0\,\mathrm{cm}$, $y = 1\,\mathrm{cm}$ and $z = 0\,\mathrm{cm}$ and has a radius of 0.5 cm. The absorption coefficient of the sphere varies from 1.5 times to 40 times the background absorption $\mu_a = 0.05\,\mathrm{cm}^{-1}$ while its scattering remains unchanged and has the same value [13] as the background transport scattering $\mu_s' = 10.0\,\mathrm{cm}^{-1}$. A comparison between the University of Pennsylvania standard data and the analytic 3D solution in case of a neglectable influence of the absorber (source and detector 1 as in Figure 2, $\mu_a^{abs} = 0.075\,\mathrm{cm}^{-1}$) showed that the time scale of the data set must be multiplied by the factor 2 what we did.

The numerical FEM parameters are adapted by a series of test simulations. The final FEM grid for handling the data series contains 2749 nodes and 5398 triangles as shown in slightly cut form in Figure 2. The domain is chosen to be about $184\,\mathrm{mm} \times 180\,\mathrm{mm}$ in size,
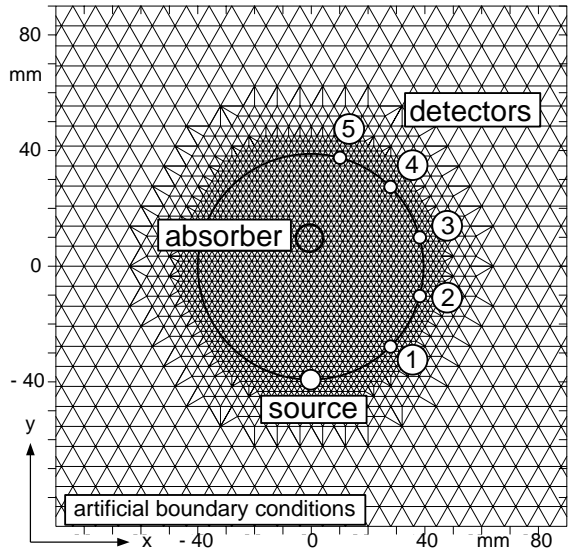
Fig. 2: FEM-grid with the measurement geometry for the source in position $x_s = 0\,\text{mm}$, $y_s = -40\,\text{mm}$.
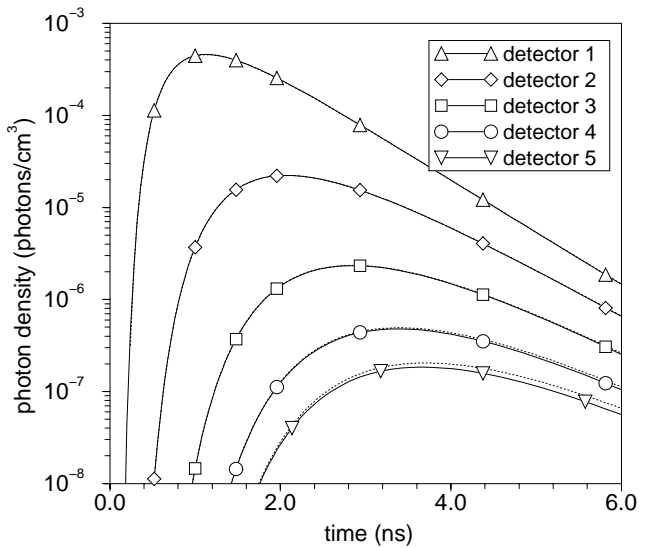
Fig. 3: Approximate 3D simulation results for the ten-fold absorber. Comparison between the simulated photon density and the University of Pennsylvania standard data set in five detector positions.

large enough for the influence of the absorber on the boundary to be neglected. The lengths in the x– and the y–direction are unequal because equilateral triangles are used. A circular section just enclosing the detector and the source positions is refined twice and the area with increased absorption is refined once again (omitted in Figure 2). Time steps are made from an initial $0.02\,\text{ns}$ to a final $0.06\,\text{ns}$. In each step of the iterative reconstruction algorithm, a new triangulation is executed which takes the current position of the detected absorber into consideration. In this way, we get a highly accurate solution which takes about $8\,\text{s}$ on a DEC computer with a $275\,\text{MHz}$ processor.

A comparison between the approximate 3D solution and the data from the University of Pennsylvania in the five detector positions corresponding to Figure 2 is illustrated in Figure 3. The absorber at $x^{abs} = 0\,\text{mm}$, $y^{abs} = 10\,\text{mm}$ with a radius of $r^{abs} = 5\,\text{mm}$ has an absorption coefficient of $\mu_a^{abs} = 0.5\,\text{cm}^{-1}$, i.e. ten times the background absorption. The photon densities are relatively given as response of a normalized light source with strength equal to 1. For detectors 1 till 3 a good agreement is found, but for detectors 4 and 5 small differences appear as the curves are more strongly influenced by the absorber. The reason is that 3D approximation is rougher here.

For the simulation of an error of measurement we assume that a TCSPC technique is applied. It provides Poisson distributed numbers of counted photons with a mean value λ_l for each time channel $(t_l - \frac{1}{2}T_c, t_l + \frac{1}{2}T_c)$, where T_c is the channel width [17]. For large numbers of counts, this distribution can be approximated by a normal distribution with a mean value λ_l and the variance λ_l. For the test data we assume that the relative uncertainty in the maximum of the curves for each set has the same value which serves as the parameter of noise intensity.

6

III. THE INVERSE PROBLEM

A. Algorithm

The formulation of our inverse reconstruction procedure allows for the a priori information that a single absorber has to be detected in a homogeneous surrounding medium. A generalization to cover several absorbers or scatterers, even if the number is unknown, can be made. An absorber in a plane is described by four parameters: the coordinates x^{abs} and y^{abs}, the radius r^{abs} and the absorption coefficient in the centre point μ_a^{abs}. Together with the background absorption μ_{a0}, five parameters are to be identified which for the following description we denote by the vector of unknown parameters $\mathbf{p}$.

The basic strategy of the fit consists in an iterative correction of the parameters and can be demonstrated by a formal procedure:

$$
\begin{array}{lll}
\mathbf{1.} & \text{Choose an initial guess for } \mathbf{p}. \\
\\
\mathbf{2.} & \text{Solve the forward problem, i.e. compute } \mathbf{\Phi}^{sim}(\mathbf{p}). \\
\\
\mathbf{3.} & \text{Compare } \mathbf{\Phi}^{sim}(\mathbf{p}) \text{ with } \mathbf{\Phi}^{mes}; \\
& \text{if} \quad \|\mathbf{\Phi}^{sim}(\mathbf{p}) - \mathbf{\Phi}^{mes}\|_w \quad \text{small} \quad \text{then} \quad \text{go to } \mathbf{5}. \\
\\
\mathbf{4.} & \text{Correct } \mathbf{p} \quad \text{and} \quad \text{go to } \mathbf{2}. \\
\\
\mathbf{5.} & \text{End}
\end{array}
\tag{12}
$$

Here the full information contained in time-resolved measurements for the image reconstruction is used as in previous versions [2–4,15,18].

With the choice of a weighted l_2-norm to compare the vectors of simulated and measured data, the optimization problem (12) becomes a weighted least squares problem

$$
\begin{aligned}
||\mathbf{\Phi}^{sim}(\mathbf{p}) - \mathbf{\Phi}^{mes}||_w^2 &= \sum_{k=1}^{m}\sum_{j=1}^{n_k}\sum_{i=1}^{q_{jk}} w_{ijk}|\Phi_k^{sim}(\boldsymbol{x}_{jk}, t_{ijk}, \mathbf{p}) - \Phi_k^{mes}(\boldsymbol{x}_{jk}, t_{ijk})|^2 \\
&= \sum_l |F_l(\mathbf{p})|^2 = min \ !
\end{aligned}
\tag{13}
$$

where Φ^{sim} is the simulated and Φ^{mes} the measured photon density, m is the number of sources, n_k the number of detectors of the $k-$th source, and q_{jk} the number of times corresponding to the $j-$th detector of the source k. Considering the chi-square fitting, the weights are

$$
w_{ijk} = \frac{1}{|\Phi_k^{mes}(\boldsymbol{x}_{jk}, t_{ijk})| \max_{1 \le l \le q_{jk}} |\Phi_k^{mes}(\boldsymbol{x}_{jk}, t_{ljk})|} .
$$

As expected, this inverse problem is rather ill-conditioned. The weighted least squares problem (13) is solved by the Levenberg-Marquardt method [19] of the IMSL program library.

B. Reconstruction results

First, the algorithm was tested for the two-dimensional case using data generated by our forward simulator. The measurement configuration and the test object were chosen to be the same as for the standard data. In test series, the number of sources and the absorption of the inhomogeneity were varied. 10 detectors were used in all reconstructions. The smallest number of sources was two and the weakest absorber had a 1.5-fold absorption compared to background absorption. In all cases the absorber was found to be accurate as regards size, position and absorption coefficient. In a second test, the attempt of reconstruction from the 3D data using the 2D forward model failed. The differences between 2D and 3D simulation results dominated over the absorber information.

Next, the algorithm was tested using the approximate three-dimensional forward model described in Section II A. The time-of-flight curves of a varying number of sources (12, 6, 4, 3 or 2) at 10 detector positions for each source were used. We define a detection to be successful if the centre of the recognized absorber lies in the area of the expected absorber. For our test examples, an absorber is considered to be successfully recognized, if the distance d between the centre of the detected absorber and that of the expected absorber is smaller than 5 mm. The radii and the absorption coefficients may differ from the expected values, because in the 3D approximation the absorbing sphere is replaced by a long cylinder (cf. Section II A). These parameters were, therefore, not used for the evaluation of the reconstruction result. In all cases, the background absorption was very well reproduced.

First we consider the original standard data series without additional noise. Surprisingly, the results essentially do not depend on the number of sources. The values of the identified parameters for the 2-fold absorber in dependence on the number of sources used are given in Table 1. The identified radii and absorption coefficients of the sphere are inaccurate, as had been expected before. This drawback will be compensated by the fact that substantial
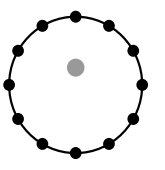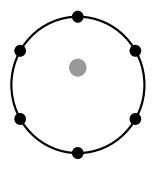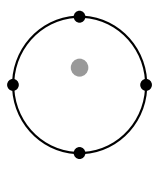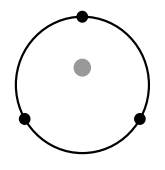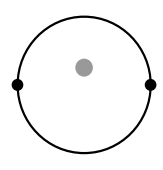
		to be	12 sources	6 sources	4 sources	3 sources	2 sources
x^{abs}	mm	0.00	-0.20	-0.08	-0.12	-0.10	-0.07
y^{abs}	mm	10.00	12.88	13.12	13.26	12.58	13.51
r^{abs}	mm	5.00	1.05	1.47	1.95	1.93	1.66
μ_a^{abs}	cm^{-1}	0.1	0.48	0.26	0.17	0.17	0.24
d	mm	0.00	2.89	3.12	3.26	2.58	3.51

Table 1: Reconstruction results for a 2-fold absorber and different number of sources and 10 detectors being used in each case by means of the original standard data series without additional noise. The four parameters of the absorber and the distance d between the centre of the detected absorber and that of the expected absorber are listed.

computational effort will be saved, because the aim of this tomographic method is in the first place the detection of a tumor at the correct position. The results obtained by fewer measurement series are comparable to those obtained from all curves available. The reason is the redundancy in the measurement information. The reduction of the number of detectors instead of the number of sources also leads to good detection results, but the computational effort is approximately proportional to the number of sources and does not depend on the number of detectors. When simultaneous measurements at several detectors are possible, the same is valid for the measuring time. Therefore, the reduction of the number of sources seems to be more advantageous. The detection of the 1.5-fold absorber failed for all configurations.
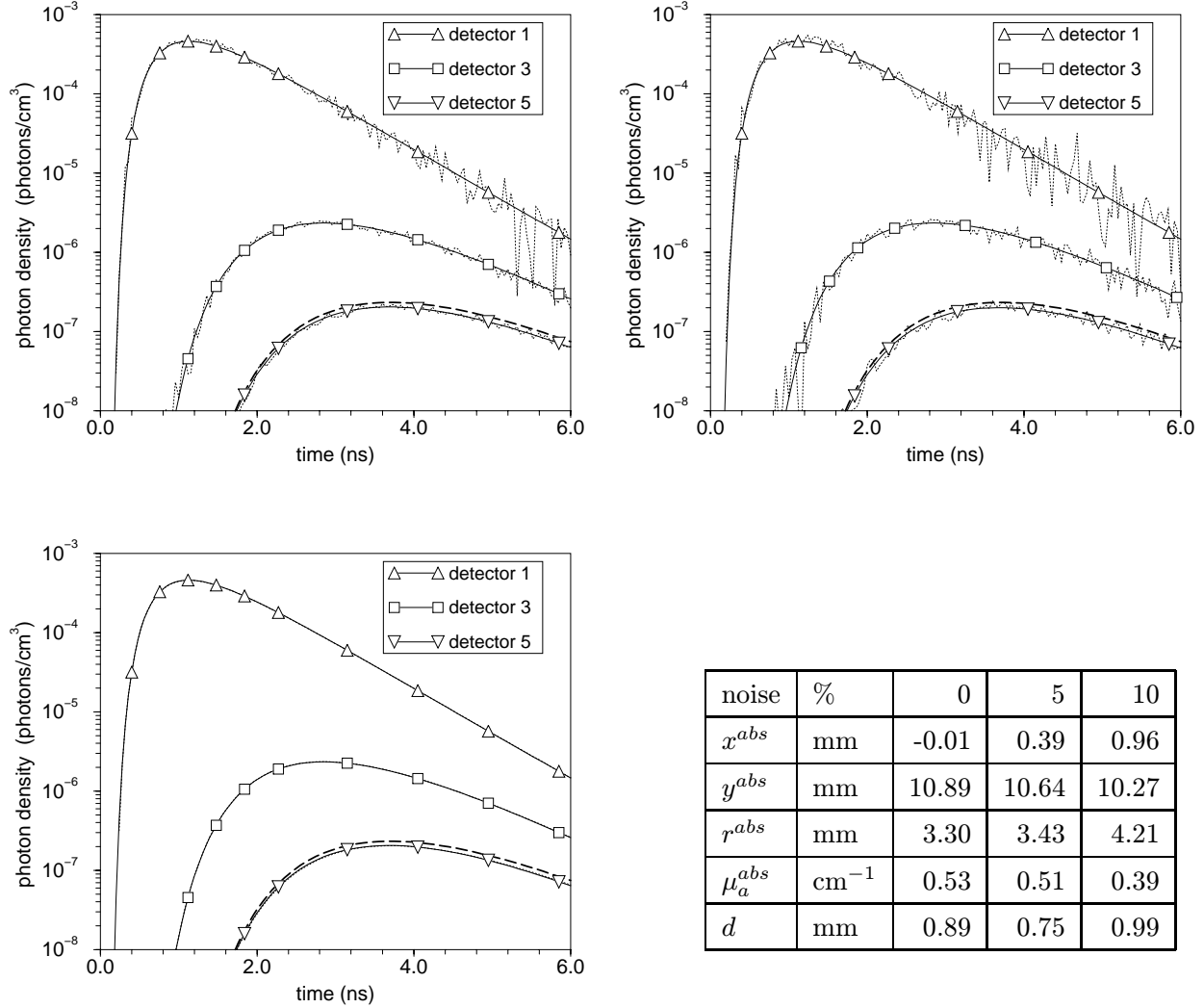

noise	%	0	5	10
x^{abs}	mm	-0.01	0.39	0.96
y^{abs}	mm	10.89	10.64	10.27
r^{abs}	mm	3.30	3.43	4.21
μ_a^{abs}	cm^{-1}	0.53	0.51	0.39
d	mm	0.89	0.75	0.99

Fig. 4: Reconstruction results. Comparison between the University of Pennsylvania standard data set for $\mu_a^{abs} = 0.5\,\mathrm{cm}^{-1}$ with additional noise (dotted line), simulated photon densities after identification using 12 sources, 10 detectors (solid line) and the densities for a homogeneous medium (dashed line). Source and detectors are chosen as in Figure 2. Top on the left 5% noise and on the right 10% noise; bottom on the left 0% noise. The values of the identified parameters are given in the table.
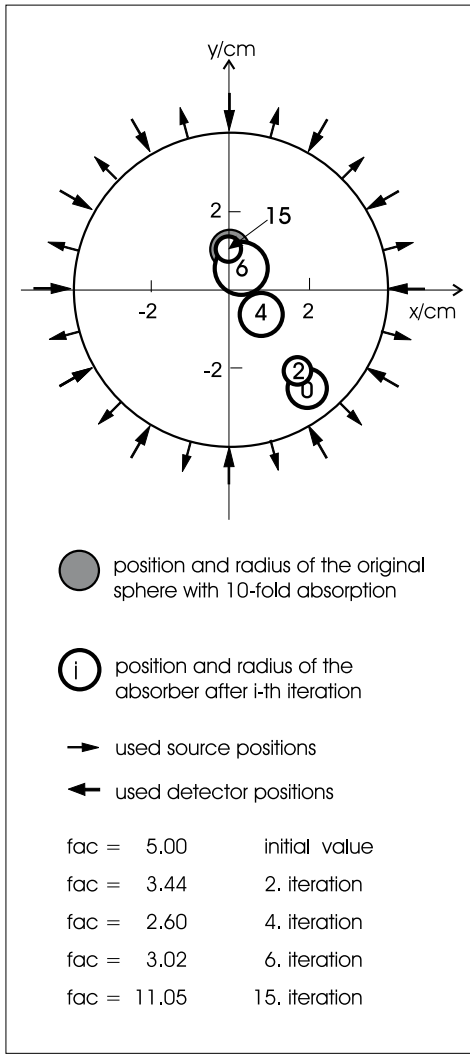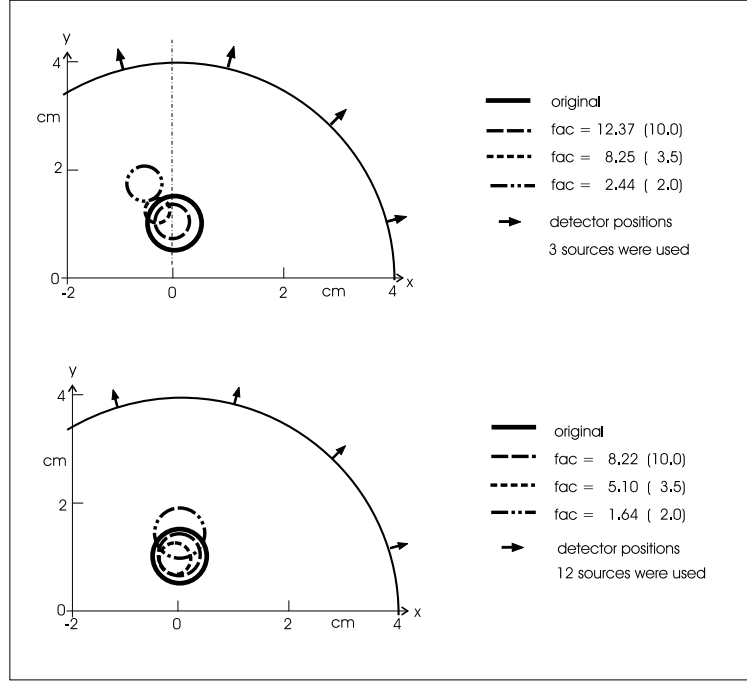
Fig. 5: Selected iteration solutions starting from a strongly unfavourable initial guess using 12 sources and 10 detectors ($fac = \mu_a^{abs}/\mu_{a0}$).

Fig. 6: Reconstruction results for different absorption coefficients μ_a^{abs} of the sphere and 10% data noise (the expected value of fac in brackets). Top: 3 sources, 10 detectors. Bottom: 12 sources, 10 detectors.

Legend for Fig. 5:

- position and radius of the original sphere with 10-fold absorption
- (i) position and radius of the absorber after i-th iteration
- → used source positions
- ← used detector positions

fac =	5.00	initial value
fac =	3.44	2. iteration
fac =	2.60	4. iteration
fac =	3.02	6. iteration
fac =	11.05	15. iteration

Fig. 6 legend (Top: 3 sources, 10 detectors):

- original
- fac = 12.37 (10.0)
- fac = 8.25 (3.5)
- fac = 2.44 (2.0)
- → detector positions
- 3 sources were used

Fig. 6 legend (Bottom: 12 sources, 10 detectors):

- original
- fac = 8.22 (10.0)
- fac = 5.10 (3.5)
- fac = 1.64 (2.0)
- → detector positions
- 12 sources were used

When noisy data are used, the situation is different. Figure 4 shows a comparison between the University of Pennsylvania standard data set for 10-fold absorption with additional 5% and 10% noise (dotted line), the simulated photon densities using the identified parameters (solid line) and the densities for a homogeneous medium without any absorber (dashed line). Time-of-flight curves of three detectors corresponding to detectors 1, 3 and 5 in Figure 2 are chosen. Here the forward simulated curves with identified parameter lie in between the noisy curves, nearly in the middle. In the absence of noise, differences between corresponding curves are hardly visible, in contrast to Figure 3. The inaccuracy of the approximate 3D model is compensated by changes of the optical parameters. The influence of the absorbing sphere on the time-of-flight curves is small. At detector positions 1 and 3 the curves graphically coincide with the homogeneous case (see Figure 4). A difference is remarkable for detector 5, where the absorber lies within the banana shape of the source-detector pair. For weaker absorbers, of course, it is even smaller. The numerical identification algorithm has to be very sensitive to these small differences to detect an inhomogeneity.

Tests with different start values for the absorber were made. The results coincide for the position of the sphere but the radius r^{abs} and absorption μ_a^{abs} somewhat differ. The reason

is the bad condition of the inverse problem. Figure 5 shows the results of the iteration steps 2, 4, 6 and the final step 15 for a ten-fold absorber starting from a strongly unfavourable initial guess (0. iteration) using 12 sources and 10 detectors. For the general test series an absorber in position (0,0) was chosen as initial guess. The reconstruction results considering 10% data noise are illustrated in Figure 6 for different absorption of the sphere (2-, 3.5- and 10-fold). As expected, the 10-fold absorber is best detected and the 2-fold worst. The deviation from the original position for the 2-fold absorber is unacceptable to a successful reconstruction when 3 sources are used only (top). In case of weak absorbers the number of sources has a clear influence. On the other hand, the reduction of the data noise improves the image reconstruction, too.

Figure 7 gives a summary of selected reconstruction results. For greater clarity, only the distance d for several absorbers (2-fold to 10-fold) is represented as it is characteristic for the success of the reconstruction procedure. The results for the undisturbed data are included for comparison. For 12 sources with 10 detectors each (Figure 7, on top), the absorber is found in almost all cases, with the exception of the 2-fold absorber and 15% noise. Signal processing by an appropriate filter for the noisy data improves the situation, and all absorbers can be successfully detected. Surprisingly, a filter deteriorates the result in some tests. The reason is that the filter error may decrease the information of the data depending on the random selection of the deviation. The good detection results, despite data noise, were achieved because of the strong redundancy of data. The reduction of the number of sources to three sources noticeably worsens recognition (Figure 7 bottom). The noise is limited to 10% here. Data filtering improves the results in all cases but does not successfully help in three examples (2.5-fold absorber and 10% noise, 2-fold absorber and 5% or 10% noise, respectively). Corresponding results for 4 or 6 sources lie in between.

Finally let us note, that all reconstruction results given here are related to the test object and the measurement configuration used. Differences may be expected if scatterers or more than one absorber have to be identified.

IV. CONCLUSIONS

We have presented a new imaging method in the time domain for the detection of perturbations of the optical properties in nearly homogeneous media. This is the situation typical in optical mammography. A time-dependent diffusion model for the light propagation in tissue is solved by a finite-element method. The consideration of difference densities leads to a higher accuracy and a substantial reduction of the computational effort. A new approximation of the three-dimensional photon migration is introduced consisting in numerical calculations in two spatial dimensions and in multiplying with a time-dependent correction factor. Quantitative agreement is found between the approximate 3D solution and 3D standard data series. The reconstruction method is successfully applied to the 3D standard data series while the detection of test absorbers using uncorrected 2D calculations fails. The influence of the error of measurement on the reconstruction is investigated using simulated random error functions. With increasing data noise, good recognition of the absorber is more difficult. The results show that in this case a sufficient number of sources (and detectors) is important. The algorithm is adapted to the configuration in the infinite medium corresponding to the given data, but it can be generalized to cover finite objects.

11

Summarizing, it can be said that the proposed method offers new possibilities of treating 3D reconstruction problems with an acceptable computational effort.
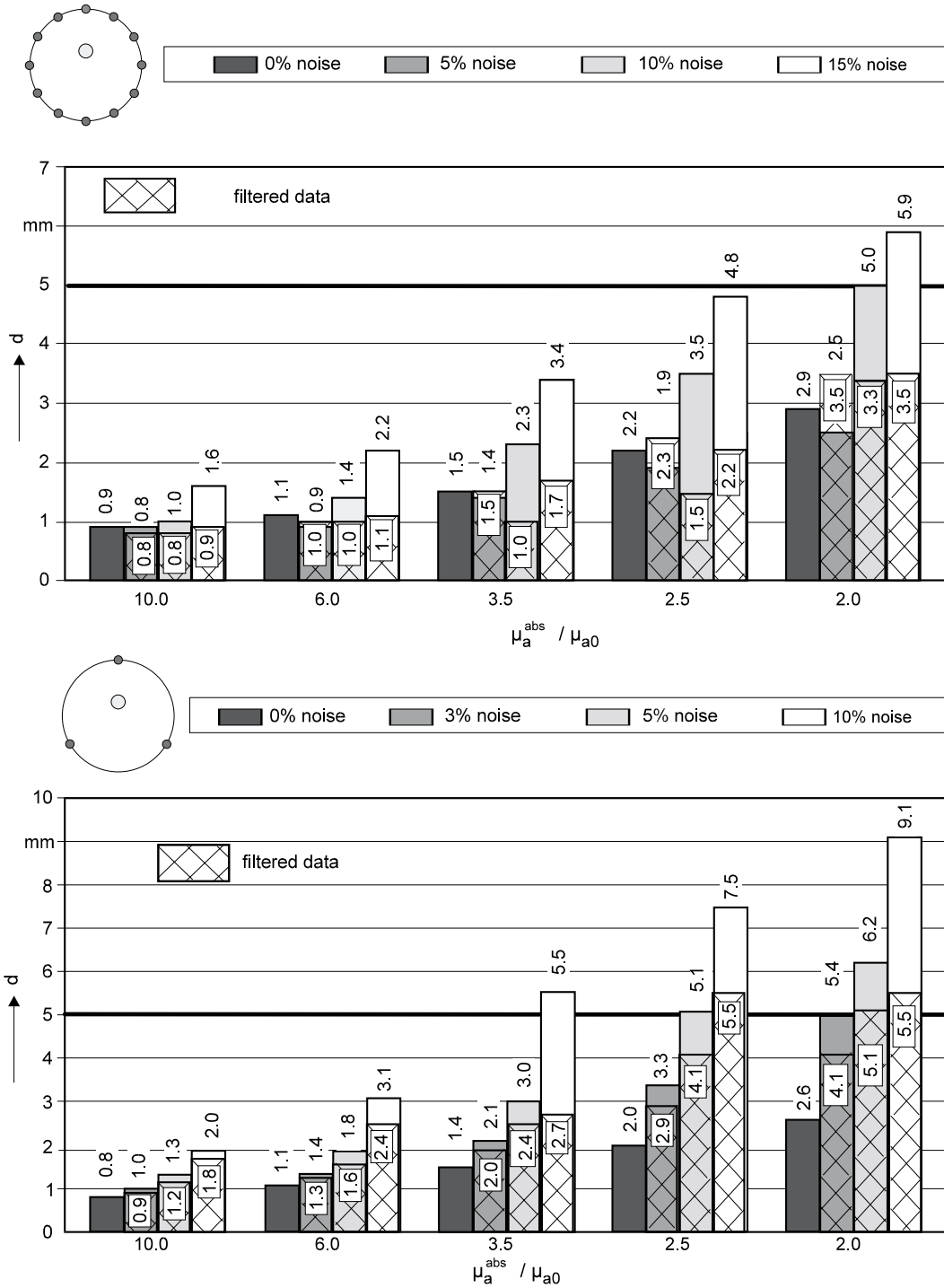

Fig. 7: Reconstruction results using noisy data. The dependence of d (distance between the centre of the detected absorber and that of the expected absorber) on the absorption of the sphere and on the noise level is illustrated. Top: 12 sources, 0%, 5%, 10%, and 15% noise. Bottom: 3 sources, 0%, 3%, 5%, and 10% noise.

ACKNOWLEDGEMENTS

---

[1] G. Müller, B. Chance, R. R. Alfano, S. Arridge, J. Beuthan, E. Gratton, M. Kaschke, B. Masters, S. Svanberg, and P. van Zee, eds., *Medical Optical Tomography: Functional Imaging and Monitoring,* SPIE Institutes, Vol. IS11, (1993).

[2] R. Model, R. Hünlich, M. Orlt, and M. Walzel, "Reconstruction algorithm for near-infrared imaging in turbid media by means of time-domain data", J. Opt. Soc. Am. A **14**, 313-324 (1997).

[3] R. Model, R. Hünlich, M. Orlt, and M. Walzel, "Image reconstruction for random media by diffusion tomography", in *Optical Tomography, Photon Migration, and Spectroscopy of Tissue and Model Media: Theory, Human Studies, and Instrumentation,* B. Chance and R. R. Alfano, eds., Proc. SPIE **2389**, 400-410 (1995).

[4] M. Orlt, M. Walzel, and R. Model, "Transillumination imaging performance using time domain data", in *Photon Propagation in Tissue,* B. Chance, D.T. Delpy, and G.J. Müller, eds., Proc. SPIE **2626**, 346-357 (1995).

[5] S. R. Arridge, M. Schweiger, M. Hiraoka, and D. T. Delpy, "Performance of an iterative reconstruction algorithm for near-infrared absorption and scatter imaging", in *Photon Migration and Imaging in Random Media and Tissue,* R. R. Alfano and B. Chance, eds., Proc. SPIE **1888**, 360-371 (1993).

[6] B.W. Pogue, M.S. Patterson, and T.J. Farrell, "Forward and inverse iterative calculations for 3-D frequency diffuse optical tomography", in *Optical Tomography, Photon Migration, and Spectroscopy of Tissue and Model Media: Theory, Human Studies, and Instrumentation,* B. Chance and R. Alfano, eds., Proc. SPIE **2389**, 328-339 (1995).

[7] M.V. Klibanow, T. R. Lucas, and R. M. Frank, "New imaging algorithm in diffusion tomography", in *Biological Imaging and Spectroscopy of Tissue: Theory, Instrumentation, Model, and Human Studies II,* D. A. Benaron and B. Chance, eds., Proc. Spie **2979**, 272- 283 (1997).

[8] A. Ishimaru, *Wave propagation in random scattering media* (Academic Press, New York, 1978).

[9] S. R. Arridge, M. Cope, van der Zee, P. J. Hillson, and D. T. Delpy, "Visualisation of the oxygenation state of brain and muscle in newborn infants by near infra-red transillumination", in *Information Processing in Medical Imaging,* S. L. Bacharach, ed. (Martinus Nijhoff, Amsterdam, 1985), 155-176.

[10] Y. Wang, J. Chang, R. Aronson, R. L. Barbour, H. L. Graber, and J. Lubowsky, "Imaging of scattering media by diffusion tomography: an iterative perturbative approach", in *Physiological Monitoring and Early Detection Diagnostic Methods*, Proc. SPIE **1641**, 58-71 (1993).

[11] S. C. Feng, F-A. Zeng, B. Chance, "Analyical perturbation theory of photon migration in the presence of a single absorbing or scattering defect sphere", in *Optical Tomography, Pho-*

ton Migration, and Spectroscopy of Tissue and Model Media: Theory, Human Studies, and Instrumentation, Proc. SPIE **2389**, 54-63 (1995).

[12] M. R. Ostermeyer and S. T. Jacques,"Perturbation theory for optical diffusion theory: a general approach for absorbing and scattering objects in tissue", in *Optical Tomography, Photon Migration, and Spectroscopy of Tissue and Model Media: Theory, Human Studies, and Instrumentation,* Proc. SPIE **2389**, 98-102 (1995).

[13] D. Boas, *Time-domain standard data series.* University of Pennsylvania, URL http://www.lrsm. upenn.edu/pmi/DATA/stand_data.html.

[14] M. Orlt, M. Walzel, and R. Model, "Influence of different kind of error on imaging results in optical tomography", in *Advanced Mathematical tools in Metrology II,* P. Ciarlini, M. Cox, F. Pavese, and D. Richter, eds., (World Scientific Singapure, New Jersey, London, Hong Kong, 1997), 277-279.

[15] R. Model and R. Hünlich, "Parameter sensitivity in near infrared imaging", in *Photon Propagation in Tissue,* B. Chance, D.T. Delpy, and G.J. Müller, eds., Proc. SPIE **2626**, 56-65 (1995).

[16] D. A. Boas, M. A. O'Leary, B. Chance, and A. G. Yodh, "Scattering of diffuse photon density waves by spherical inhomogeneities within turbid media: Analytic solution and applications", Proc. Nat. Acad. Sci. USA **91**, 4887-4891 (1994).

[17] D. V. O'Conner and D. Phillips, *Time-correlated single photon counting* (Academic Press London, Orlando, San Diego, 1984).

[18] R. Model and R. Hünlich, "Optical imaging of highly scattering media", ZAMM **76**, 483-484 (1996).

[19] J. E. Dennis, Jr., and R. B. Schnabel, *Numerical Methods for Unconstrained Optimization and Nonlinear Equations* (Prentice-Hall, Englewood Cliffs, New Jersey, 1983).